

Size-Dependent Upconversion Luminescence in Er³⁺/Yb³⁺-Codoped Nanocrystalline Ytria: Saturation and Thermal Effects

Xue Bai,^{†,‡} Hongwei Song,^{*,†} Guohui Pan,^{†,‡} Yanqiang Lei,^{†,‡} Tie Wang,[†] Xingguang Ren,[†] Shaozhe Lu,[†] Biao Dong,^{†,‡} Qilin Dai,^{†,‡} and Libo Fan^{†,‡}

Key Laboratory of Excited State Physics, Changchun Institute of Optics, Fine Mechanics and Physics, Chinese Academy of Sciences, 16 Eastern Nan-Hu Road, Changchun 130033, P. R. China, and Graduate school of Chinese Academy of Sciences

Received: January 7, 2007; In Final Form: May 7, 2007

In this paper, the upconversion luminescent properties of Y₂O₃:Er³⁺(1%)/Yb³⁺(4%) nanoparticles with different sizes (13–55 nm) and its corresponding bulk material as a function of excitation power were studied under 978-nm excitation. Red (⁴F_{9/2} → ⁴I_{15/2}), green (²H_{11/2}, ⁴S_{3/2} → ⁴I_{15/2}), and blue (²H_{9/2} → ⁴I_{15/2}) transitions were observed. The results indicated that the relative intensity of the blue as well as the red to the green increased gradually with decreasing particle size. As a function of excitation power, the slope in the ln–ln plot for the red emission changed between 2.0 and 1.0 and gradually decreased with increasing particle size, which was attributed to competition between linear decay and upconversion processes for the depletion of the intermediate excited states. As the particle size decreased to 13 nm, a three-photon populating process occurred for the green emission. As the excitation power varied in different paths, gradually increasing or gradually decreasing, a hysteresis loop appeared in the power dependence of emission intensity, which was mainly caused by a local thermal effect induced by laser irradiation. The intensity ratio of ²H_{11/2} → ⁴I_{15/2} to ⁴S_{3/2} → ⁴I_{15/2} (*R_{HS}*) varied complicatedly with excitation power, which was theoretically explained considering the thermal distribution and relaxation processes. Two novel cross-relaxation paths were proposed on the basis of the variation of *R_{HS}* under excitation at different wavelengths, 488 and 978 nm.

I. Introduction

Considerable interest has been centered on the conversion of infrared radiation to shorter wavelength by materials doped with trivalent rare-earth ions for more than 30 years.^{1,2} Up to now, various upconversion (UC) host materials have been developed and studied, such as crystals, glasses, ceramics, and so on.^{3–5} Recently, nanosized luminescent materials have attracted intensive attention. The reduction of particle size in a crystalline system can result in remarkable modifications of some of their bulk properties because of a high surface-to-volume ratio and the quantum confinement effect of nanometer materials. Phosphors in the nanoscales can exhibit novel physical properties, such as higher luminescent efficiency and better resolution of images in lighting and display.^{6,7} Taking advantage of these size-induced changes, infrared-to-visible upconversion luminescence (UCL) in nanocrystals has attracted considerable attention as a result of their potential application in some optical fields, such as infrared detection, molecule recognition, three-dimensional displays, and so forth.^{8–10}

Among the candidates of UC nanomaterials, Y₂O₃ nanocrystals (NCs) doped with Er³⁺ ions and sensitized with Yb³⁺ ions have been widely studied because not only does Y₂O₃ have high chemical durability and thermal stability,¹¹ but also the Er³⁺ ion has a favorable energy level capable of infrared pumping that closely matches the most attractive 978-nm laser

diode (LD) wavelength, which is in fair agreement with the peak wavelength of Yb³⁺ ion absorption. Capobianco et al.¹² reported the influence of particle size and Yb³⁺ concentration on conversion luminescence and observed that the decreased particle size and increased Yb³⁺ concentration resulted in increased intensity ratio of red emissions (⁴F_{9/2} → ⁴I_{15/2}) to green emissions (⁴S_{3/2}/²H_{11/2} → ⁴I_{15/2}). Serra et al. studied the low-temperature upconversion spectroscopy of the Y₂O₃:Er³⁺/Yb³⁺ nanophosphor, which showed a decrease in emission intensity with increasing temperature.¹³ Our group and Capobianco's group both reported that as the Yb³⁺ concentration was high enough, the green upconversion emissions of ⁴S_{3/2}/²H_{11/2} → ⁴I_{15/2} were dominated by a three-photon process.^{12,14} The studies on UC dynamics demonstrated that as the particle size was small enough, the energy transfer from Yb³⁺ to Er³⁺ happened less because of the improved nonradiative relaxation rate of the ²F_{7/2} → ²F_{5/2} for Yb³⁺.¹⁵ In the similar nanocrystalline system of Gd₂O₃:Er³⁺/Yb³⁺, the saturation effect and local thermal effect were observed.¹⁶ Despite the fact that some novel spectral phenomena have been observed in the nanocrystalline Y₂O₃:Er³⁺/Yb³⁺ or similar nanocrystals, few systematic studies on size-dependent UCL behavior were reported.

In this paper, the influence of particle size on UCL of Y₂O₃:Er³⁺/Yb³⁺ NCs were studied systemically. Some novel and interesting upconversion properties were reported, being the complementary results of previous studies. It was observed that not only the ratio of the red to the green but also the ratio of the blue to the green increased with decreasing particle size. In nanocrystalline Y₂O₃:Er³⁺/Yb³⁺, luminescent hysteresis loops appeared in the dependence of upconversion intensity on pump

* Corresponding author. Fax: 86-431-6176320. E-mail: songhongwei2000@sina.com.cn.

[†] Key Laboratory of Excited State Physics, Changchun Institute of Optics, Fine Mechanics and Physics, Chinese Academy of Sciences.

[‡] Graduate school of Chinese Academy of Sciences.

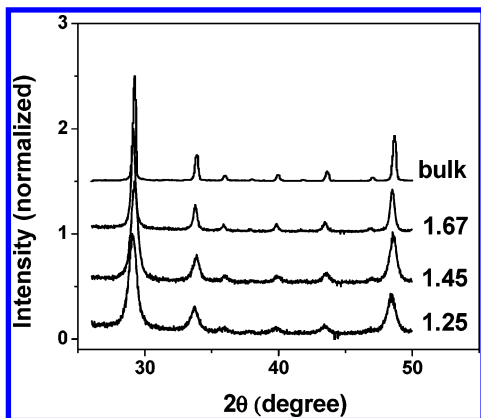


Figure 1. XRD patterns of $\text{Y}_2\text{O}_3:\text{Er}^{3+}/\text{Yb}^{3+}$ NCs prepared at different conditions.

power as the pump light changed via two different paths: increasing gradually or decreasing gradually.

II. Experiments

A. Sample Preparation. The Y_2O_3 NCs doped with 1 mol % of Er_2O_3 and 4 mol % of Yb_2O_3 were prepared by a solution combustion synthesis procedure. In the preparation, Y_2O_3 , Er_2O_3 , and Yb_2O_3 (in the molar ratio of 1:0.01:0.04) were dissolved in nitric acid, and glycine was dissolved in distilled water; then the two kinds of solution were mixed together to form the precursor. Details of the synthesis have been given elsewhere.¹⁷ The particle size was controlled by adjusting the molar ratio of glycine to metal nitrate (G/N), which had affected the combustion temperature in the reaction. In the preparation, the values of G/N were controlled to be 1.25, 1.45, and 1.67. To improve the crystallinity of the nanocrystalline powders and eliminate redundant nitrate, all of the resultant $\text{Y}_2\text{O}_3:\text{Er}^{3+}/\text{Yb}^{3+}$ was annealed at 500 °C for 2 h. In comparison, the bulk $\text{Y}_2\text{O}_3:\text{Er}^{3+}/\text{Yb}^{3+}$ powders were prepared by annealing the mixed Y_2O_3 , Er_2O_3 , and Yb_2O_3 powders (in the molar ratio of 1:0.01:0.04) at 1100 °C for 6 h.

B. Measurements and Characterization. Crystal structure and particle size were obtained by X-ray diffraction (XRD) using a Cu target radiation resource. In UCL experiments, a 978-nm diode laser having a power maximum of 2 W was used to pump the samples. The visible emissions were collected using a F-4500 fluorescence spectrometer. In the measurements of temperature-dependent luminescence, the samples were put into a liquid nitrogen cycling system, in which the temperature varied in the range of 150–600 K. A continuous 488-nm light that came from an argon laser was used as the excitation source. The fluorescence was measured by a UV-Lab Raman Infinity (made by Jobin Yvon Company) with a resolution of 2 cm^{-1} .

The crystal structure and particle size were obtained by X-ray diffraction (XRD) patterns, as shown in Figure 1. According to JCPDS standard cards, all the nanoparticles exhibit pure cubic structure. From the top to the bottom in Figure 1, the XRD patterns become broader and broader, suggesting that the crystalline size decreases gradually. The peaks shift a little ($\sim 0.1^\circ$) to the small diffraction angle, implying that the lattice constant becomes smaller due to the effect of strain. Taking account of the effect of instrumental broadening, the average crystalline size of the NCs was estimated by the Scherrer formula to be ~ 13 , 27, and 55 nm, respectively, for the samples of $G/N = 1.25$, 1.45, and 1.67. In the calculation, we have neglected the effect of strain on the broadening of XRD patterns, because the strain effect should not be remarkable as judged

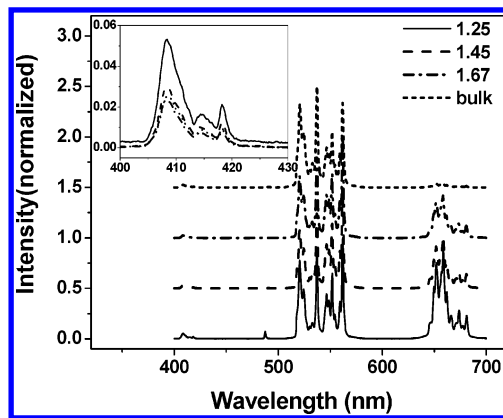


Figure 2. Visible UCL luminescence spectra in various $\text{Y}_2\text{O}_3:\text{Er}^{3+}/\text{Yb}^{3+}$ NCs and bulk materials (the pump power is 845 mW).

according to the shift of XRD patterns. Note that previously we also measured the scan electron micrograph (SEM) images of some Y_2O_3 NCs prepared by the combustion process, which was well in accordance with the estimated values by XRD patterns.¹⁸ The nanoparticles observed from TEM images tended to aggregate. This should have little influence on the calculation of crystalline size by the Scherrer formula because aggregation does not influence crystallinity.

III. Results

A. UCL Spectra in Nanocrystalline $\text{Y}_2\text{O}_3:\text{Er}^{3+}/\text{Yb}^{3+}$ Powders with Different Sizes. Figure 2 shows the normalized UCL spectra in Y_2O_3 powders with different sizes under 978-nm excitation. In the spectra the green emissions were observed in the range of 500–580 nm, corresponding to the $^2\text{H}_{11/2}$, $^4\text{S}_{3/2} \rightarrow ^4\text{I}_{15/2}$ transitions, while the red lines were observed between 640 and 690 nm, corresponding to the $^4\text{F}_{9/2} \rightarrow ^4\text{I}_{15/2}$ transitions. As shown in the inset of Figure 2, the enlarged UCL spectra in the blue region display emissions assigned to the $^2\text{H}_{9/2} \rightarrow ^4\text{I}_{15/2}$ transitions, ranging from 400 to 425 nm. The locations of these three transitions in Y_2O_3 powders with different sizes are identical, suggesting that the crystal fields surrounding the Er^{3+} and Yb^{3+} ions are reasonably similar and not affected by the size of the particles. It is clearly observed that not only the relative intensity of the red ($^4\text{F}_{9/2} \rightarrow ^4\text{I}_{15/2}$) to the green ($^4\text{S}_{3/2}, ^2\text{H}_{11/2} \rightarrow ^4\text{I}_{15/2}$), but also that of the blue ($^2\text{H}_{9/2} \rightarrow ^4\text{I}_{15/2}$) to the green ($^4\text{S}_{3/2}, ^2\text{H}_{11/2} \rightarrow ^4\text{I}_{15/2}$) increases with decreasing particle size. It should be noted that the relative increase for the red emission has been frequently described in some previous literature, while that for the blue emission has not been observed yet. Different populating paths induce the variation of relative intensity of different transitions and will be described later.

B. Power-Dependence of UCL. For nearly any upconversion mechanism, the visible output intensity (I_v) will be proportional to some power (n) of the infrared excitation (I_{IR}) power:¹²

$$I_v \propto I_{\text{IR}}^n$$

where n is the number of IR photons absorbed per visible photon emitted. In the present case, the result is different. A slope equal to approximately 2 indicates that upconversion occurs via a two-photon process. Figure 3, parts a and b, shows the logarithmic plots of the emission intensity as a function of excitation power, respectively, for the green and red emissions in various samples. It is interesting to observe that the slope (n) in the \ln – \ln plot varies considerably with the particle size of the samples. For the green emission, the values of n were determined to be 2.66 ± 0.05 , 2.23 ± 0.05 , 2.01 ± 0.06 , and 1.87 ± 0.06 , respectively,

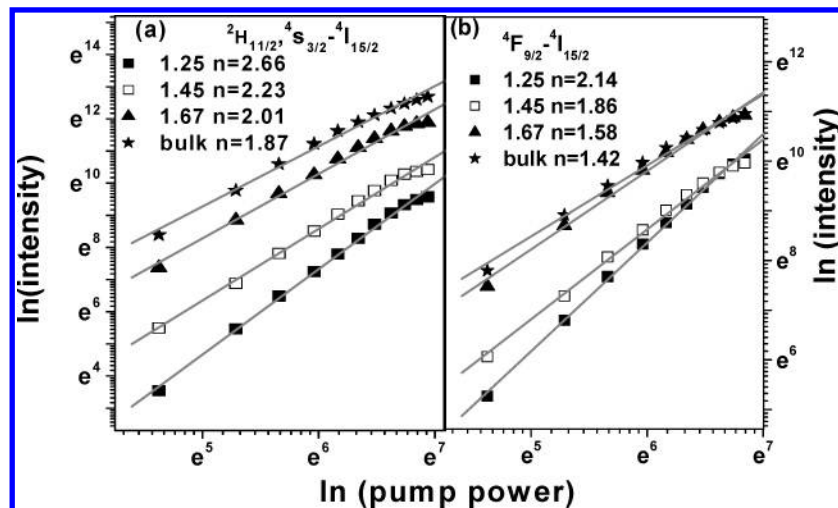


Figure 3. Plot (ln–ln) of emission intensity versus excitation power in different size particles.

in the 13-, 27-, and 55-nm NCs and in the bulk. For the red emission, the values of n were determined to be 2.14 ± 0.03 , 1.86 ± 0.04 , 1.58 ± 0.05 , and 1.42 ± 0.05 , respectively, in the 13-, 27-, and 55-nm NCs and in the bulk NCs. Obviously, the values of n increased with a decrease in the size of the samples, and the slopes of the red emission are smaller than that of the green emission in all the samples. A larger value than 2 suggests that a three-photon process should be involved for populating the green level. In principle, the slope (n) in the ln–ln plot of the green emission should be 3 for a three-photon UCL process. However, the thermal effect will decrease the slope in general, because as the excitation density was high enough, the strong absorption led the sample temperature at the irradiated region to increase, inducing a thermal effect and which will lead to the quenching of UCL. If the thermal effect could be avoided, the slopes should be larger than the present experimental values. For the green emission, the slope should be close to 3, which demonstrates that the corresponding UCL results from a three-photon process. Our previous results indicated that as the Yb³⁺ concentration was high enough (10% in molar ratio), the three-photon process was dominant for populating the green level $^4S_{3/2}/^2H_{11/2}$.¹⁴ The present result further indicates that the populating process strongly depends on particle size. The smaller the particle size is, the easier the three-photon process for the green is. It can be also observed that as the excitation power increases to a certain value (1 W), the UCL intensity deviates from a linear relationship.

As the excitation power varies, the intensity ratio (R_{HS}) of $^2H_{11/2} \rightarrow ^4I_{15/2}$ to $^4S_{3/2} \rightarrow ^4I_{15/2}$, also changes obviously. Figure 4a shows the intensity ratio of $^2H_{11/2} \rightarrow ^4I_{15/2}$ to $^4S_{3/2} \rightarrow ^4I_{15/2}$ as a function of excitation power in various samples. It can be seen that in the bulk, R_{HS} increases solely with the increase of excitation power. It varies rapidly as the excitation power is less than 1 W and grows slowly as the power surpasses 1 W. The variation of R_{HS} in NCs demonstrates a distinctive difference in comparison to the bulk. It increases with increasing excitation power initially, then approaches a maximum at a certain power (~ 1 W), and then decreases as the excitation power increases continuously.

The decrease in the slope of UPL intensity versus pump power with increasing power can be explained well by the “saturation” process. However, this conclusion can be not available for the fact that I_{UCL} decreases as the incident power is high enough (I_{UCL} decreases with the increasing excitation power in the NCs as shown in Figure 5), and the hysteresis

loop phenomenon of the emission intensity. We suggest that this can be attributed to thermal quenching of UCL caused by the absorption of the 978-nm lights. For Er³⁺ ions, the energy separation between the nearest excited states $^2H_{11/2}$ and $^4S_{3/2}$ is only several hundred wavenumbers, the population distribution on $^2H_{11/2}$ and $^4S_{3/2}$ should be dominated by thermal distribution. Therefore, the intensity ratio (R_{HS}) of $^2H_{11/2} \rightarrow ^4I_{15/2}$ to $^4S_{3/2} \rightarrow ^4I_{15/2}$ should be sensitive to temperature, and the R_{HS} is a critical parameter to study the thermal effect in NCs under the exposure of the 978-nm diode laser.

Furthermore, in order to exclude the effects of thermal damage on our samples, we studied the evolution of UCL intensity in the dark after being irradiated for 20 min by 978-nm light of 1.5 W, as shown in Figure 4b. It is found that the UCL intensity increased slowly and nearly recovered to its initial value as the irradiation light was shut off for 15 min, indicating that the irradiation did not induce thermal damage.

C. Luminescence Hysteresis Loops. Figure 5 shows the green emission intensity as a function of incident power in different samples. The up-traces show the green emission intensity as the incident power is gradually increased, while the down-traces display the intensity as the incident power is gradually decreased. In the up-traces, we can see that the emission intensities of NCs increase quickly at the original time, then approach to a saturation value and finally decrease. In the down-traces, the emission intensities decrease solely with the decreasing power. Distinct hysteresis loops are thereby formed. The photoluminescence displays a similar bistability phenomenon. For the red and blue emissions, similar hysteresis loops have also been observed in the Y₂O₃:Er³⁺/Yb³⁺ NCs. However, it is not a strict intrinsic bistability phenomenon as described in the previous references, which is dominated by the nonlinear emission processes caused by the coupling of Yb³⁺–Yb³⁺ pairs.²⁰ In the bulk powder, the area of the loop is obviously smaller than that in the NCs as shown in the inset of Figure 5, which will be discussed in detail in section IV.

IV. Discussion

A. Populating and Photoluminescence Processes. The UCL mechanism and population processes in Er³⁺/Yb³⁺-codoped systems are presented in Figure 6.²¹ The red and green UCL both occur via a two-step energy transfer from the Yb³⁺ to the Er³⁺. First, the Er³⁺ ion is excited from the ground state $^4I_{15/2}$ to the excited state $^4I_{11/2}$ via energy transfer (ET) of neighboring

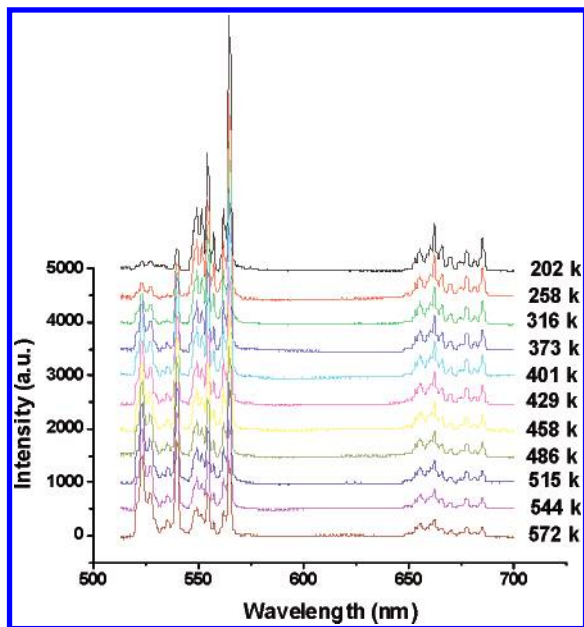


Figure 7. Visible UCL luminescence spectra in 55-nm NCs at different temperatures.

proportional to the excitation power density (P^1) when the upconversion was the dominant mechanism in the Er³⁺/Yb³⁺-codoped system.¹⁶ For any two-photon process, the intensity of an UCL that is excited by the sequential absorption of two photons has a dependence of P^α on absorbed pump power density P , with $1 < \alpha < 2$.

As shown in Figure 3, the slopes of the red emission are smaller than that of the green emission in all the samples, which can be attributed to the difference of the intermediate level between the green and the red emission. The intermediate level of the green emission is $^4I_{11/2}$, while that of the red emission is $^4I_{13/2}$. The energy separation between $^4I_{11/2}$ and $^4I_{13/2}$ is about 3600 cm^{-1} , while that of the $^4I_{13/2}$ and $^4I_{15/2}$ is about 7000 cm^{-1} .¹² In the Y₂O₃ NCs, a large number of OH⁻ and CO₃²⁻ bonds were involved, with vibrational energies of 3350 and 1500 cm^{-1} , respectively, which can bridge the nonradiative relaxation of $^4I_{11/2} \rightarrow ^4I_{13/2}$ more effectively than the nonradiative relaxation of $^4I_{13/2} \rightarrow ^4I_{15/2}$. Therefore in the $^4I_{11/2}$ level, the linear decay is dominant because the effective nonradiative relaxation of $^4I_{11/2} \rightarrow ^4I_{13/2}$ increases the linear decay processes, leading the total linear decay rate of $^4I_{11/2}$ to be larger than the upconversion rate. As a consequence, the slope of the green emission is close

to ~ 2 . On the other hand, the upconversion is the dominant depletion mechanism for $^4I_{13/2}$, thus the slope of the red emission is close to 1. As the size of the samples decreases, the rate of the multiphonon relaxation becomes larger due to surface contamination. Thus the process of linear decay becomes dominant, which is the main factor leading the slopes of the green/red emission to increase with decreasing particle size. Note that as the particle size decreases to a certain degree, the three-photon process occurs also for populating the green levels, which also leads to the increase of the slope.

C. Thermal Effect. In order to discuss the thermal effect caused by the exposure of 978-nm diode laser in UCL processes, the downconversion luminescence (DCL) under 488-nm excitation was performed at various temperatures ($77\text{--}570\text{ K}$). In the experiment, the power of the 488-nm excitation light is about 1 mW , which is much lower than the power of 978-nm excitation light in UCL and the absorption of Er³⁺ at 488 nm is much lower than the absorption of Yb³⁺ at 978 nm, thus the thermal effect can be neglected.

Figure 7 shows the emission spectra under 488-nm excitation at various temperatures. We can see that the green emissions of $^4S_{3/2} \rightarrow ^4I_{15/2}$ and the red emissions of $^4F_{9/2} \rightarrow ^4I_{15/2}$ decrease rapidly with increasing temperature in the studied temperature range, while the intensity of $^2H_{11/2} \rightarrow ^4I_{15/2}$ increases with increasing temperature. This result can be attributed to the competition between the thermal excitation and nonradiative relaxation for the two green levels. The total green emission intensity ($^4S_{3/2} \rightarrow ^4I_{15/2} + ^2H_{11/2} \rightarrow ^4I_{15/2}$) decreases a little with the increase of temperature (see Figure 8a). The intensity ratio of $^2H_{11/2} \rightarrow ^4I_{15/2}$ to $^4S_{3/2} \rightarrow ^4I_{15/2}$ as a function of temperature in the 55-nm NCs is shown in Figure 8b. It is interesting to see that the intensity ratio increases rapidly with increasing temperature and does not approach a maximum as excited by a 978-nm diode laser in the studied temperature range.

As mentioned in section III, because of low-energy separation between $^2H_{11/2}$ and $^4S_{3/2}$, the population distribution on $^2H_{11/2}$ and $^4S_{3/2}$ should be dominated by thermal distribution. Thus the population ratio of $^2H_{11/2} \rightarrow ^4I_{15/2}$ to $^4S_{3/2} \rightarrow ^4I_{15/2}$ can be written as

$$R'_{HS} = \frac{N_1}{N_2} = \alpha e^{-\Delta E/kT} \quad (1)$$

where α is a constant, N_1 and N_2 are the populations of the levels $^2H_{11/2}$ and $^4S_{3/2}$, respectively, ΔE is the energy difference between the two levels ($^2H_{11/2}$ and $^4S_{3/2}$), between which the nonradiative relaxation happens, k is Boltzmann's constant, and

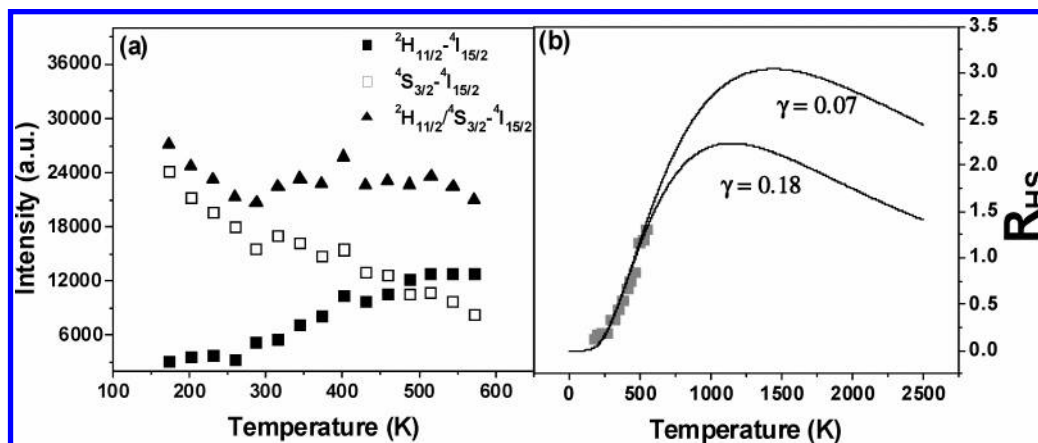


Figure 8. (a) The intensity of $^2H_{11/2} \rightarrow ^4I_{15/2}$, $^4S_{3/2} \rightarrow ^4I_{15/2}$, and $^2H_{11/2}/^4S_{3/2} \rightarrow ^4I_{15/2}$ as a function of temperature; (b) the intensity ratio of $^2H_{11/2} \rightarrow ^4I_{15/2}$ to $^4S_{3/2} \rightarrow ^4I_{15/2}$ as a function of temperature.

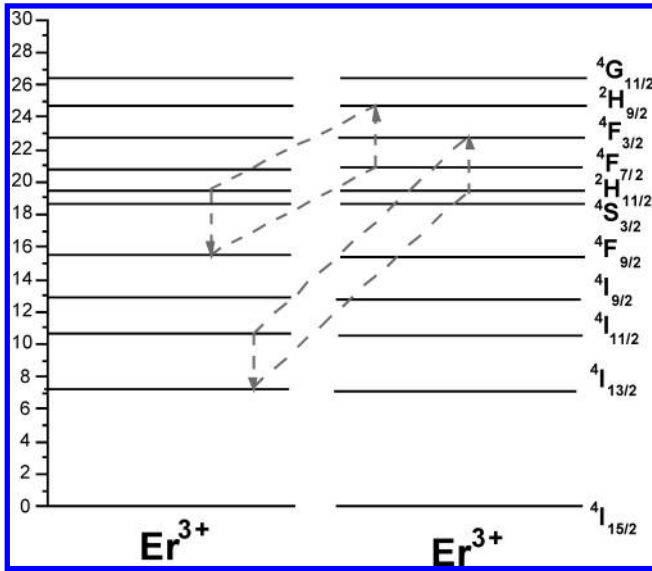


Figure 9. Schematic of the cross-relaxation mechanisms in $\text{Y}_2\text{O}_3:\text{Yb}^{3+}/\text{Er}^{3+}$ NCs following 978-nm excitation.

T is the absolute temperature. The intensity ratio R_{HS} can be written as

$$R_{HS} = \frac{I_{2\text{H}_{11/2}}}{I_{4\text{S}_{3/2}}} = \frac{N_1 R_1 \tau_1}{N_2 R_2 \tau_2} = \frac{N_1 R_1 (R_2 + W_{\text{NR}2})}{N_2 R_2 (R_1 + W_{\text{NR}1})} \quad (2)$$

where τ_1 and τ_2 represent the lifetime of level $2\text{H}_{11/2}$ and $4\text{S}_{3/2}$, respectively, $W_{\text{NR}1}$ and $W_{\text{NR}2}$ are the nonradiative transition rates from $2\text{H}_{11/2}$ and $4\text{S}_{3/2}$ to the down levels, respectively, R_1 and R_2 are the radiative rates of $2\text{H}_{11/2} \rightarrow 4\text{I}_{15/2}$ and $4\text{S}_{3/2} \rightarrow 4\text{I}_{15/2}$. According to eq 2, and assuming $W_{\text{NR}1} \approx W_{\text{NR}}$ (W_{NR} are the nonradiative transition rates of $\text{H}_{11/2} \rightarrow 4\text{S}_{3/2}$), the R_{HS} can be written as

$$R_{HS} = \frac{1 + \frac{W_{\text{NR}2}}{R_2}}{1 + \frac{W_{\text{NR}}}{R_1}} R'_{HS} \quad (3)$$

where $W_{\text{NR}2}$ is considered as a constant, because the energy separation between $4\text{S}_{3/2}$ and its neighboring down-level $4\text{F}_{9/2}$ is much larger than that of $2\text{H}_{11/2} \rightarrow 4\text{S}_{3/2}$. The variation of $W_{\text{NR}2}$ with temperature can be neglected in comparison to that of W_{NR} . As is well-known, the nonradiative transition rate in the rare-earth ions for multiphonon relaxation can be written as¹⁸

$$W_{\text{NR}} = W_{\text{NR}}(0)[1 + \langle n \rangle]^{\Delta E/\hbar\omega} \quad (4)$$

where $W_{\text{NR}}(0)$ is the nonradiative relaxation rate at 0 K, $\hbar\omega$ is the photon energy, and $\langle n \rangle = (1/\exp(\hbar\omega/kT) - 1)$ is the phonon density. On the basis of eqs 3 and 4, the population ratio of R_{HS} can be deduced as

$$R_{HS} = \frac{\beta \exp(-\Delta E/kT)}{1 + \gamma[1 - \exp(-\hbar\omega/kT)]^{-\Delta E/\hbar\omega}} \quad (5)$$

with

$$\beta = \left(1 + \frac{W_{\text{NR}2}}{R_2}\right) \alpha$$

and

$$\gamma = 1 + \frac{W_{\text{NR}}}{R_1}$$

The experimental data are fitted well by eq 5 as shown in Figure 8b. In the calculation, $\hbar\omega$ is chosen to be 377 cm^{-1} , which is a typical vibration mode of the Y_2O_3 host. Two phonons of 377 cm^{-1} exactly match the energy separation between $2\text{H}_{11/2}$ and $4\text{S}_{3/2}$ ($\sim 740 \text{ cm}^{-1}$). By fitting, β and γ were determined to be 13 and 0.18, respectively. The theoretical calculation is very consistent with the experimental result under the excitation of 488 nm in the range of 77–570 K. From Figure 8b, we can also observe that as the temperature is high enough (1139 K), an intensity maximum appears in the temperature dependence. As the temperature increases continuously, the intensity ratio decreases gradually with temperature. This result suggests that the thermal excitation contributes dominantly to the population distribution between the two green levels when the temperature is lower; when the temperature is high enough ($\sim 1100 \text{ K}$), the nonradiative relaxation from $2\text{H}_{11/2}$ to $4\text{S}_{3/2}$ is comparable to the thermal excitation. The theoretical dependence of R_{HS} on temperature can quantitatively explain the variation of R_{HS} with temperature. Note that in the NCs, R_{HS} is always smaller than that in the bulk powders at any excitation power. This can be explained according to Figure 8b by the curves selecting different values of γ . The increased γ means that the nonradiative transition rate in the nanoparticles increases, which is in accordance with the results in some previous references.²³

It is surprising to observe that the intensity ratio of $2\text{H}_{11/2} \rightarrow 4\text{I}_{15/2}$ to $4\text{S}_{3/2} \rightarrow 4\text{I}_{15/2}$ pumped by the 488-nm light is obviously larger than that pumped by the 978-nm light, which can be attributed to different energy transfer channels. We suggest that the energy transfer decreases the emission of $2\text{H}_{11/2} \rightarrow 4\text{I}_{15/2}$. Under the 978-nm excitation and as the excitation power is high enough, the $2\text{I}_{11/2}$ and the $2\text{F}_{7/2}$ are populated effectively by one-step or two-step energy transition processes. Because the energy separations between $4\text{I}_{11/2} \rightarrow 4\text{I}_{13/2}$ and $2\text{H}_{11/2} \rightarrow 4\text{F}_{3/2}$ match closely, the same as that between $4\text{F}_{7/2} \rightarrow 2\text{H}_{9/2}$ and $2\text{H}_{11/2} \rightarrow 4\text{F}_{9/2}$, the cross-relaxation of $2\text{I}_{11/2} + 2\text{H}_{11/2} \rightarrow 4\text{I}_{13/2} + 4\text{F}_{3/2}$ and $4\text{F}_{7/2} + 2\text{H}_{11/2} \rightarrow 2\text{H}_{9/2} + 4\text{F}_{9/2}$ probably happens between the two neighboring Er^{3+} ions (see Figure 9). When the excitation power intensity increases, the populating of the direct excitation level $2\text{I}_{11/2}$ and $4\text{F}_{7/2}$ is more effective, which intensively enhances the cross-relaxation mentioned above, resulting in the decreased ratio of $2\text{H}_{11/2} \rightarrow 4\text{I}_{15/2}$ to $4\text{S}_{3/2} \rightarrow 4\text{I}_{15/2}$.

V. Conclusions

Size-dependent UCL properties of cubic $\text{Y}_2\text{O}_3:\text{Er}^{3+}(1\%)/\text{Yb}^{3+}(4\%)$ nanoparticles prepared by solution combustion were studied under 978-nm excitation. The results indicate that the relative intensity of the blue ($2\text{H}_{9/2} \rightarrow 4\text{I}_{15/2}$) transition to the green ($4\text{S}_{3/2}/2\text{H}_{11/2} \rightarrow 4\text{I}_{15/2}$) one gradually increases with decreasing particle size, like the relative intensity of the red ($4\text{F}_{9/2} \rightarrow 4\text{I}_{15/2}$) transition. As a function of excitation power (0–2 W), the slope in the \ln – \ln plot gradually decreases with increasing particle size, for both the red and the green transitions. For the red transition, the slope varies from 2.0 to 1.0 as the particle size increases, which is attributed to competition between linear decay and upconversion processes for the depletion of the intermediate excited states. For the green

emission, the slope is close to 3.0 as the particle size decreases to ~13 nm, suggesting the occurrence of a three-photon process.

In addition, it is observed that the intensity ratio of $^2H_{11/2} \rightarrow ^4I_{15/2}$ to $^4S_{3/2} \rightarrow ^4I_{15/2}$ increases with the increasing power originally, then approaches a maximum at a certain power (~1 W), and then decreases as the excitation power increases continuously. This is theoretically explained by considering both the thermal population and the nonradiative relaxation processes of $^2H_{11/2}$ and $^4S_{3/2}$. Under the 978-nm excitation, the intensity ratio of $^2H_{11/2} \rightarrow ^4I_{15/2}$ to $^4S_{3/2} \rightarrow ^4I_{15/2}$ obviously decreases in contrast to that under the 488-nm excitation, which is attributed to the cross-relaxation processes on $^2H_{11/2}$.

As the excitation power varies in different paths, a hysteresis loop appears in the power dependence of emission intensity. These two facts are mainly attributed to the local thermal effect induced by the exposure to a 978-nm laser diode. In conclusion, the particle size can considerably modify the population channels and emission processes in Y₂O₃:Er³⁺/Yb³⁺-codoped nanocrystals.

Acknowledgment. The authors are thankful for financial support by the National Natural Science Foundation of China (Grants 10374086 and 10504030) and the Talent Youth Foundation of JiLin Province (Grant 20040105).

References and Notes

- (1) Johnson, L. F.; Geusic, J. E.; Guggenheim, H. J.; Kushida, T.; Singh, S. *Appl. Phys. Lett.* **1963**, *15*, 48.
- (2) Kano, T.; Yamamoto, H.; Otomo, Y. *J. Electrochem. Soc.* **1973**, *119*, 1561.
- (3) Takahashi, M.; Lzuki, M.; Kanno, F.; Kawamoto, Y. *J. Appl. Phys.* **1998**, *83*, 392.

- (4) Zhou, J.; Moshary, F.; Gross, B. M.; Aark, M. F.; Ahmed, G. A. *J. Appl. Phys.* **2004**, *96*, 237.
- (5) Garcia, A. S.; Serna, R.; Castrc, M. J.; Afonso, C. N. *Appl. Phys. Lett.* **2004**, *84*, 2151.
- (6) Hong, K. S.; Meltzer, R. S.; Bihari, B.; Williams, D. K.; Tissue, B. M. *J. Lumin.* **1998**, *234*, 76.
- (7) Bhargara, R. N.; Gallagher, D.; Hong, X.; Nurmikko, A. *Phys. Rev. Lett.* **1994**, *72*, 416.
- (8) Hebert, T.; Wannemacher, R.; Lenth, W.; Macfarlane, R. M. *Appl. Phys. Lett.* **1990**, *57*, 1727.
- (9) Mita, Y.; Hiram, K.; Ando, N.; Yamamoto, H.; Shionoya, S. *J. Appl. Phys.* **1993**, *74*, 4703.
- (10) Downing, E.; Hesselink, L.; Ralston, J.; Macfarlane, R. *Science* **1996**, *273*, 1185.
- (11) Williams, D. K.; Bihari, B.; Tissue, B. M.; Mchale, J. M. *J. Phys. Chem. B* **1998**, *102*, 916.
- (12) Vetrone, F.; Boyer, J. C.; Capobianco, J. A. *J. Appl. Phys.* **2004**, *96*, 661.
- (13) Pires, A. M.; Serra, O. A. *J. Appl. Phys.* **2005**, *98*, 063529.
- (14) Song, H. W.; Sun, B. J.; Wang, T.; Lu, S. Z.; Yang, L. M.; Chen, B. J.; Wang, X. J.; Kong, X. G. *Solid State Commun.* **2004**, *132*, 409.
- (15) Song, H.; Xia, H.; Sun, B.; Lu, S.; Liu, X.; Yu, L. *Chin. Phys. Lett.* **2006**, *23*, 474.
- (16) Lei, Y.; Song, H.; Yang, L.; Yu, L.; Liu, Z.; Pan, G.; Bai, X.; Fan, L. *J. Chem. Phys.* **2005**, *123*, 174710.
- (17) Yang, L. M.; Song, H. W.; Yu, L. X.; Liu, Z. X.; Lu, S. Z. *J. Lumin.* **2006**, *116*, 101.
- (18) Song, H.; Chen, B.; Peng, H.; Zhang, J. *Appl. Phys. Lett.* **2002**, *81*, 1776.
- (19) Capobianco, J. A.; Vetrone, F.; Alesio, T. D.; Tessari, G.; Speghini, A.; Bettinelli, M. *Phys. Chem. Chem. Phys.* **2000**, *2*, 3203.
- (20) Hehlen, M. P.; Kuditcher, A.; Rand, S. C.; Luthi, S. R. *Phys. Rev. Lett.* **1999**, *82*, 30.
- (21) Song, H. W.; Xia, H. P.; Sun, B. J.; Lu, S. Z.; Liu, Z. X.; Yu, L. X. *Chin. Phys. Lett.* **2006**, *23*, 474.
- (22) Pollnau, M.; Gamelin, D. R.; Luthi, S. R.; Gudel, H. U. *Phys. Rev. B* **2000**, *61*, 3337.
- (23) Bai, X.; Song, H. W.; Yu, L. X.; Yang, L. M.; Liu, Z. X.; Pan, G. H.; Lu, S. Z.; Ren, X. G.; Lei, Y. Q.; Fan, L. B. *J. Phys. Chem. B* **2005**, *109*, 15236.